Preparation, Characterization, and Biological Activity of Stability-Enhanced Polyethyleneimine-Conjugated Gold Nanoparticles (Au-PEI@NIST) for Biological Application

Tae Joon Cho
Vincent A. Hackley
Feng Yi
David A. LaVan
Vytas Reipa
Alessandro Tona
Bryant C. Nelson
Christopher M. Sims
Natalia Farkas

NIST

**National Institute of
Standards and Technology**

U.S. Department of Commerce

NIST Special Publication 1200-29

Preparation, Characterization, and Biological Activity of Stability-Enhanced Polyethyleneimine-Conjugated Gold Nanoparticles (Au-PEI@NIST) for Biological Application

Tae Joon Cho
Vincent A. Hackley
Feng Yi
David A. LaVan
Materials Measurement Science Division
Material Measurement Laboratory

Vytas Reipa
Alessandro Tona
Bryant C. Nelson
Biosystems and Biomaterials Division
Material Measurement Laboratory

Christopher M. Sims
Materials Science and Engineering Division
Material Measurement Laboratory

Natalia Farkas
[1]*Theiss Research*
7411 Eads Ave, La Jolla, CA 92037
[2]*Microsystems and Nanotechnology Division*
Physical Measurement Laboratory

Publications in the SP 1200 subseries include written procedural methods in the design and implementation of experiments that ensure successful replication of results by others. Publications may include detailed procedures, lists of required equipment and instruments, information on safety precautions, the calculation of results and reporting standards.

Foreword

This NIST Special Publication (SP) is one in a series of NIST SPs that address research needs articulated in the National Nanotechnology Initiative (NNI) Environmental, Health, and Safety Research Strategy published in 2011.(1) This Strategy identified a Nanomaterial Measurement Infrastructure (NMI) as essential for science-based risk assessment and risk management of nanotechnology-enabled products as pertaining to human health, exposure, and the environment. NIST was identified as the lead federal agency in the NMI core research area of the Strategy. This research area includes development of measurement tools for the detection and characterization of engineered nanomaterials in nanotechnology-enabled products. A process for polyethyleneimine-conjugated gold nanoparticle preparation, the focus of this SP, is established through an optimization study towards an effective and systematic approach. This work is relevant for nanotechnology environment, health, and safety (NanoEHS) considerations, and for biological applications.

Abstract

In this special publication, we report on a modified synthetic process that results in a stable suspension of Au-polyethyleneimine nanoparticles, Au-PEI@NIST. Synthesized materials were characterized using an orthogonal approach that includes dynamic light scattering (DLS), UV-Vis absorbance (UV-Vis), transmission electron microscopy (TEM), atomic force microscope (AFM), and thermogravimetric analysis (TGA). Very importantly, the end-product in this study demonstrated excellent colloidal stability in multiple aqueous environments including over a wide pH and temperature range of physiological relevance. The product also exhibited long-term storage stability under ambient conditions. Furthermore, the cytotoxicity of Au-PEI@NIST was investigated using the CHO K1 cell line and exhibited dose proportional toxicity, which suggested potential for use as a positive control in nanotoxicology studies. The results and stringent testing regimen point toward an effective and sustainable approach that can serve as a clarified starting point for the development of more complex conjugates for applications in nanomedicine area.

Table of Contents

List of Tables

List of Figures

Fig. 12. Reproducibility of Au-PEI@NIST prepared using the optimized condition in 100 mL scale reactions; UV-Vis absorbance spectra are shown. The inset lists the values of λ_{max} and the average z-average (hydrodynamic) diameter for each replicate reaction.

Fig. 13. MTS cell viability assay results for CHO K1 cell line after 24 h exposure to Au-PEI@NIST nanoparticles (blue), CeO_2 NP (red), and $CdSO_4$ (green, as a positive control).

1. Introduction

Gold nanoparticles (AuNPs) remain one of the most important platforms for investigating biological applications of nanomaterials due in part to their general biocompatibility.(2, 3) In particular, positively charged (cationic) AuNPs are of interest in terms of biochemical activities related to their cellular uptake(4-6) and gene delivery/transfection(7-13) efficacies. These properties are related to the charge properties of cationic AuNPs, which drive preferred interaction with negatively charged biological entities. Among the many cationic conjugates available, polyethyleneimine (PEI) is one of the most studied polycations due to its attractive intrinsic characteristics including water-solubility, complex formation with metal ions(14) and/or anionic polyelectrolytes,(15) and, most interestingly, gene transfection/delivery efficiency for advanced biological applications.(16) Thus, Au-PEI conjugates, as a result of combination between AuNPs and PEI, are expected to produce synergic effects; inducing (1) enhanced efficacy for nano-biological applications due to their bio-compatibility (from Au) and (2) active interaction with biological entities (from PEI). Although the results of polyethyleneimine-conjugated gold nanoparticles (Au-PEIs) with respect to their preparation(17-21) have been discussed at length in the literature, a knowledge gap still exists regarding the role of PEI structure, size (relative molar mass, M_r) and preparation methods with respect to the response and stability in different media. Recently, Cho et. al at NIST reported(22, 23) the synthesis of Au-PEI by a reduction method that was systematically investigated to elucidate the optimal conditions to produce stable, high quality Au-PEI, and therein, the method was subjected to multi-parametric analysis of key factors including molar mass and PEI structure (branched or linear), PEI/Au molar ratio, concentration of reactants, and reaction temperature and time. End products obtained by the optimized condition exhibited high reduction yield of Au^{III} to Au^0, narrow size distributions with appropriate size-associated surface plasmon resonance (SPR) band, shape uniformity, high positive surface charge and functionality, and outstanding colloidal stability through the insightful characterizations using orthogonal analysis. In this report, in order to practically utilize the optimized Au-PEI as a biologically applicable positively charged nanomaterial, the optimized condition of Au-PEI preparation was modified and scaled-up along with its characterization of critical physicochemical properties related to biological application. The reported findings and precise methods provide useful information for the nano-biotechnology research community for improved understanding of specific aspects of the preparation process on the product properties.

2. Principal and scope

Au-PEI can be highly stable under physiological conditions making the system an ideal candidate for bio-medical applications (e.g., drugs/targeting species, sensing/diagnostic components) (4-13). Therefore, an optimized synthetic method for preparing highly qualified and stable Au-PEI has been developed. After evaluating many published methods to synthesize Au-PEI,(17-21) and finding poor reproducibility or limited acceptable properties for biomedical applications, we initiated an investigation to better understand the controlling factors and to yield a facile and robust methodology. Based on the previous results by Cho *et al.* at NIST,(22, 23) in this special publication, we report on a modified synthetic process that results in a stable suspension of Au-PEI nanoparticles, hereafter Au-PEI@NIST; 25 nm nominal hydrodynamic size in 100 mL batch scale at approximately 500 mg/L concentration.

Synthesized materials were characterized using an orthogonal approach that includes dynamic light scattering (DLS), UV-Vis absorbance (UV-Vis), transmission electron microscopy (TEM), and atomic force microscope (AFM). Most importantly, the end-product in this study demonstrated excellent colloidal stability avoiding particle agglomeration and/or aggregation in multiple aqueous environments (particularly in isotonic media). Stability was demonstrated over a wide pH and temperature range of physiological relevance. The product also exhibited long-term storage stability under ambient conditions. In addition, the mass ratio of Au/PEI was evaluated by thermogravimetric analysis (TGA) to assess the coverage of PEI on the gold surface. Furthermore, the cytotoxicity of Au-PEI@NIST was investigated using the CHO K1 cell line and exhibited dose proportional toxicity, which suggested potential for use as a positive control in nanotoxicology studies. The results and stringent testing regimen point toward an effective and sustainable approach that can serve as a clarified starting point for the development of more complex conjugates for targeted drug delivery, bio-diagnostics or investigations of interactions between nanoparticle and biological entities in applications such as gene transfection/genome editing.

3. Materials and equipment

3.1. Materials

3.1.1. Gold(III) chloride hydrate ($HAuCl_4 \cdot 3H_2O$, ACS reagent, e.g., Sigma-Aldrich, St. Louis, MO)

3.1.2. Branched PEI with 25kDa of molar mass (bPEI 25kDa, e.g., Sigma-Aldrich)

3.1.3. Ultrapure biological grade deionized (DI) water; at least 18.0 MΩ•cm resistivity, passed through a 0.2 μm sterile filter

3.1.4. 0.05 mol/L HCl (aq) and 0.05 mol/L NaOH (aq) reagent grade solutions for pH adjustment (e.g., Sigma-Aldrich)

3.1.5. Phosphate buffered saline (PBS) 10x solution (e.g., HyClone Laboratories, Logan, UT; Catalog No. SH30258.02) with 0.067 mol/L (PO_4^{3-}), calcium and magnesium free, passed through a 0.2 μm sterile filter following dilution

3.1.6. Dulbecco's Modified Eagle's Medium (DMEM); 4.5 g/L glucose and sodium pyruvate without L-glutamine and phenol red, sterile (e.g., Mediatech, Inc., Manassas, VA; Catalog No. 17-205-CV)

3.1.7. Bovine serum albumin (BSA); reagent grade (99+ % purity), lipid and IgG free, powder (e.g., SeraCare Life Science, Gaithersburg, MD; Product Code AP-4510-80)

3.1.8. Silicon oil for oil bath (e.g., Sigma-Aldrich)

3.1.9. Mica substrates (e.g., Ted Pella, Redding, CA; AFM Mica discs)

3.1.10. 0.1% poly-L-lysine (PLL, e.g., Sigma-Aldrich)

3.1.11. Chinese hamster ovary CHO K1 cells (e.g., ATCC, Manassas, VA)

3.1.12. Iscove's modified Dulbecco's modified medium, IMDM (e.g., Gibco, Carlsbad, CA), 10 % volume fraction fetal bovine serum, FBS (Gibco), 1 % volume fraction, penicillin-streptomycin (100 units/mL, and 100 μg/mL)

3.1.13. CellTiter 96 AQueous One Solution Cell Proliferation Assay (MTS) (e.g., Promega, Madison, WI)

3.1.14. d < 25 nm size of cerium(IV) oxide (CeO_2) nanoparticles (e.g., Sigma-Aldrich)

3.2. Equipment

3.2.1. 3-neck round bottom flask, 250 mL

3.2.2. Reflux condenser

3.2.3. Thermometer (non-mercury liquid-in glass; -10 °C to 150 °C)

3.2.4. Magnetic stirrer/hot plate

3.2.5. Oil bath (e.g., VWR, Radnor, PA; Instatherm)

3.2.6. Variable energy transformer for bath temperature control

3.2.7. Ultrafiltration kit (stirred cell; e.g., Millipore, Burlington, MA; Amicon, 250 mL, regenerated cellulose membrane, MWCO = 100 kDa).

3.2.8. Dynamic light scattering (DLS)/Zeta potential instrument (e.g., Malvern Panalytical, Westborough, MA; Zetasizer Nano ZS)

3.2.9. Zeta potential measurement cell (e.g., Malvern Panalytical; dip cell ZEN1002)

3.2.10. Ultraviolet-visible spectrophotometer (UV-Vis) (e.g., Perkin-Elmer, Waltham, MA; Lambda 750 with 8+8 cell holder/recirculated water jacket)

3

3.2.11. Optical quality cuvettes (quartz, glass, or disposable (polymethylmethacrylate; PMMA)) for UV-Vis and (quartz, glass or disposable PMMA or polystyrene) for DLS measurements; same cuvette can be used for both measurements if compatible

3.2.12. Transmission Electron Microscope (TEM; e.g., FEI, Hillsboro, OR; Titan 80–300 analytical TEM)

3.2.13. 200 mesh Carbon-coated copper TEM grid (e.g., Ted Pella Inc., Redding, CA)

3.2.14. Atomic Force Microscope (AFM; e.g., Veeco, Plainview, NY; MultiMode AFM and Nanoscope IV controller)

3.2.15. AFM probes (e.g., Bruker, Camarillo, CA; OTESPA R3)

3.2.16. pH meter and appropriate pH electrode (e.g., Mettler Toledo, Columbus, OH; InLab Semi-Micro Combination pH electrode)

3.2.17. Temperature controllable recirculating bath (e.g., VWR, Model 1160-S)

3.2.18. Analytical balance with readability to 0.1 mg (e.g., Mettler Toledo, MS 104S)

3.2.19. Calibrated pipettes and sterile disposable tips covering (0.020 to 5.00) mL range; adjustable volume pipettes are recommended

3.2.20. 5-mL and 10-mL transport tubes (e.g., Axygen Scientific, Union City, CA; sterile polypropylene tubes with screw caps)

3.2.21. Lyophilizer (freeze-dryer) (e.g., Labconco, Kansas City, MO; FreeZone6)

3.2.22. 96-well plate photometer microtiter plate reader (e.g., BioTek, Winooski, VT; Synergy mX)

3.2.23. Incubator, 37 °C ± 1 °C, humidified, 5 % CO_2/air

3.2.24. Multichannel pipette (at least 8 position), with 200 µl volume/pipette

3.2.25. Class II Type A2 biological safety cabinet

3.2.26. Thermogravimetric Analysis (TGA; e.g., NETZSCH, Burlington, MA; STA 449 F1 Jupiter)

4. General aspects of protocol

4.1. Synthesis of Au-PEI@NIST

The apparatus for Au-PEI@NIST synthesis was set up inside a chemical fume hood. A three-neck round bottom flask equipped with a thermometer and a stir bar is set in the oil bath. To 100 mL of aqueous $HAuCl_4$ (2.5 mmol/L; 50 mg of Au^{III}) in the round bottom flask, 10 mL of aqueous bPEI 25 kDa (10 % mass fraction; 1 g) is added at room temperature (≈ 23 °C) and the reaction mixture is then heated to 80 °C with moderate stirring (≈ 12 hertz or 700 rpm). The reaction mixture takes ≈ 1 h to reach 80 °C and is then stirred for an additional 3 h[††]. The oil bath is then removed to allow the reaction mixture is to cool down to ambient temperature. The reaction medium – including product, unbound PEI and reaction byproducts – is then purified using a stirred cell ultrafiltration. In this step, the reaction medium is reduced from 100 mL to (10 to 20) mL, then backfilled with DI water to about 100 mL. This purification cycle is repeated 4 times with the final volume of Au-PEI@NIST suspension adjusted to ≈ 100 mL with DI water yielding an Au concentration of ≈ 500 mg/L.

4.2. Measurements

DLS measurement procedures used in this protocol and for validation and demonstration follow the National Institute of Standards and Technology (NIST) – Nanotechnology

---

[††] Note: The relationships between target temperature/duration time to reach target – and/or the difference between temperature of oil bath and reaction mixture in flask – should be established prior to synthesis with the specific experimental setup

Characterization Laboratory (NCL) protocol(24) (freely available online) with z-average sizes (diameter) reported as the mean of no less than five measurements plus or minus one standard deviation. Disposable optical quality cuvettes were used for DLS measurements. Zeta potential measurements were performed using the same instrument with a palladium dip cell and by applying the Smoluchowski approximation for thin double layers; results are reported as the mean of no less than three measurements plus or minus one standard deviation. UV-Vis spectra were collected using UV-transparent optical quality cuvettes with a 1 cm path-length and requiring 1 mL to fill the light path of the UV-Vis spectrometer. All DLS and UV-Vis measurements were conducted at 20 °C ± 0.1 °C except thermal stability tests. Sample temperature for UV-Vis measurements was controlled using a water circulator combined with an appropriate cell-holder jacket. DLS temperature was controlled by an on-board Peltier device.

Uncertainty analysis: Error bars and uncertainty intervals expressed in this work, unless otherwise noted, represent one standard deviation of 3 to 5 replicate measurements or replicate synthetic experiments, as appropriate.

Procedures for TEM, AFM, and TGA measurements are described below in Sec. 5.1.2., 5.1.3., and 5.4, respectively.

4.3. Stability tests
The essential stability test of synthesized Au-PEI@NIST were conducted by following protocols in the NIST Special Publication 1200-26.(25)

4.4. Test sample preparation
Samples and test media were prepared, diluted and combined in a Class II, Type A2 Biosafety Cabinet (e.g., Labconco, Purifier Logic series) to protect both worker and sample from contamination and to maintain sterility. While not required for this protocol, the use of such a device is highly recommended. For DLS and UV-Vis measurements, the final concentration of Au-PEI in test suspensions, referred to here as the '*test concentration*', should be in the range from about (5 to 50) mg/L. To conduct stability comparison tests of Au-PEI in different media, the concentration of sample in each medium should be identical within the recommended range for test concentration.

4.5. Safety
This document does not intend to address all safety concerns associated with this protocol. It is the responsibility of the user to establish appropriate safety practices according to local requirements or regulatory limitations.

5. Protocols (OR procedures) for the characterization of critical physico-chemical properties of Au-PEI@NIST

5.1. Size measurements
5.1.1. Hydrodynamic size by DLS
Place 100 µL of prepared Au-PEI@NIST suspension into an optical quality cuvette and add 900 µL of DI water to adjust the concentration to ≈ 50 mg/L (dilution factor (f) = 10). Place the cuvette into the DLS instrument and measure according to the DLS protocol.(24) Figure 1 shows an example analysis of Au-PEI@NIST product, where the measured size (mean = 24.2

nm $\pm$ 0.2 nm) is the z-average diameter (d_z; obtained by application of the cumulants method, which assumes a single Gaussian mode), which represents the hydrodynamic size of the gold colloids including the gold core and surface shell (e.g., ligands and entrained or adsorbed water).
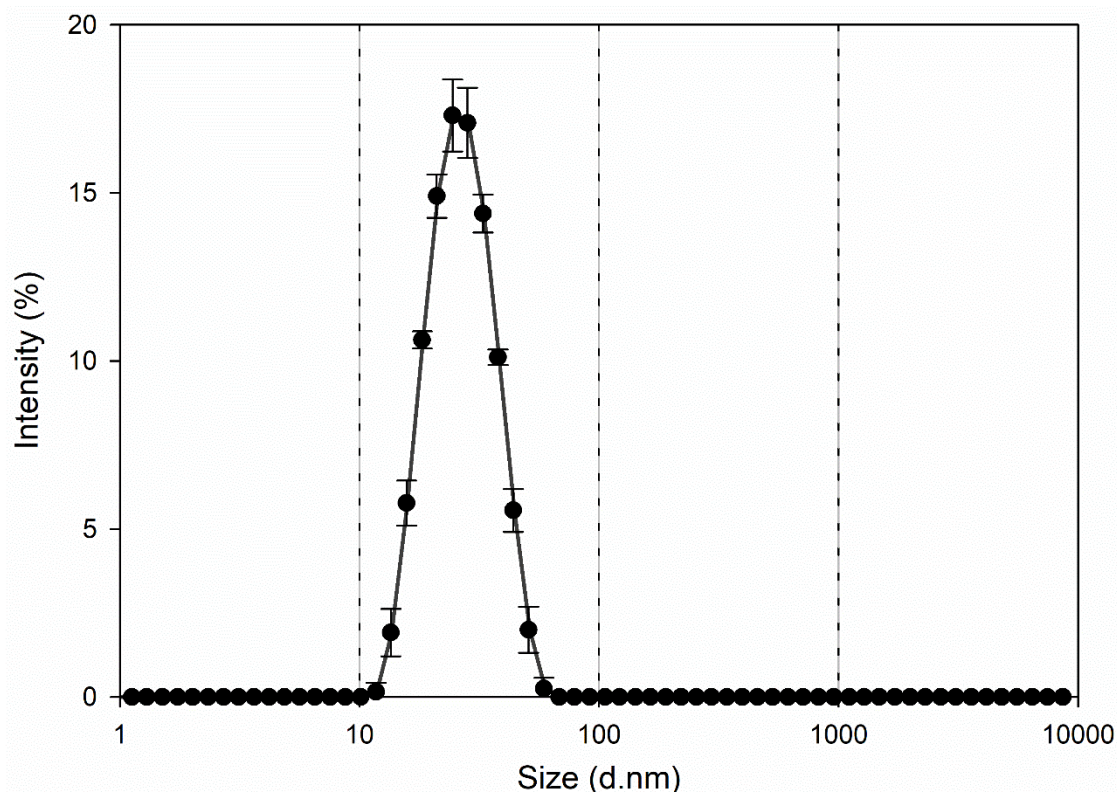
Fig. 1. Example intensity-weighted size distribution for Au-PEI@NIST by DLS. For DLS measurement, sample was first diluted in DI water ($f = 10$).

5.1.2. Core diameter by TEM

Deposit (drop cast) 10 μL of diluted Au-PEI sample ($f = 10$ in DI water) onto a carbon-coated copper TEM grid and allow to dry prior to imaging. Representative TEM images are acquired at an accelerating voltage of 300 kV. Automated particle size analysis of the TEM images is performed using Fiji(26) (a distribution of ImageJ(27)) and a processing script modified from a previously written macro.(28) Briefly, the script determines the outer boundary of each particle, then measures the number of pixels within that boundary, from which an equivalent spherical diameter is calculated using the pixel resolution (pixels/nm) obtained from the scale bar after an initial calibration (by using the TEM's image metadata for pixel-to-nm calibration). Particles that touch each other or the edge of the image are excluded from the analysis. Particles are analyzed from 5 regions of the TEM grid, with 361 individual particles measured. A representative TEM image, the differential size distribution, and the cumulative undersize distribution of the Au-PEI@NIST particles measured by TEM are shown in Figure 2. Particle sizes ranged from 3.7 nm to 16.5 nm with a mean diameter and one standard deviation of (11.8 $\pm$ 1.8) nm. The median diameter (d_{50}), obtained from the TEM statistics (as determined from the cumulative undersize distribution), is 12.0 nm, in strong agreement with the mean diameter within the uncertainty bound of one standard deviation.

6
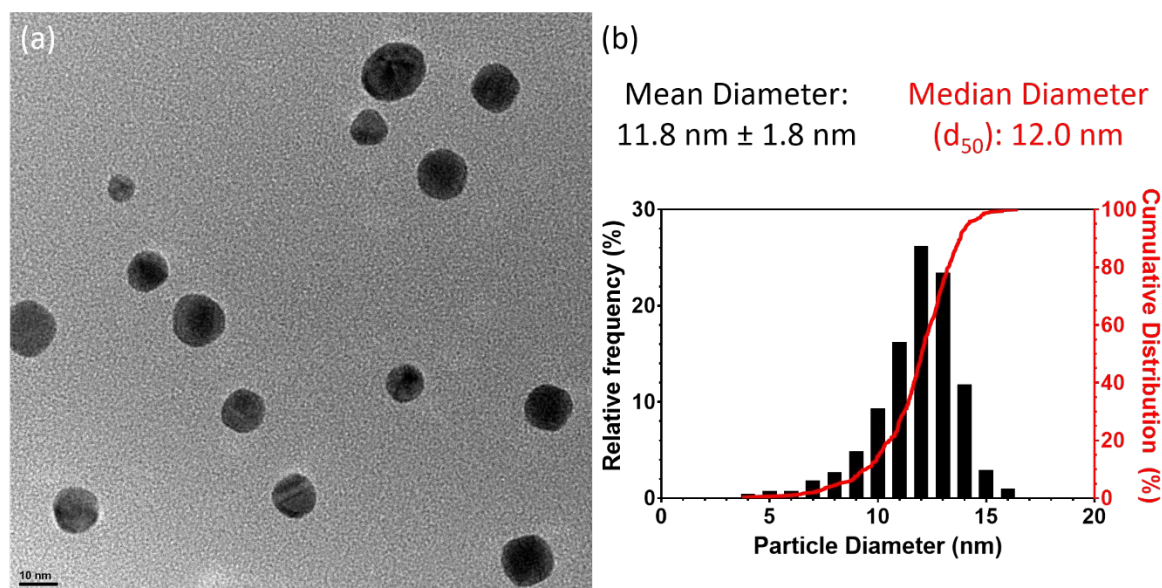
Fig. 2. (a) Representative TEM image of Au-PEI@NIST included in size analysis. Scale bar is 10 nm. (b) Differential size distribution and cumulative undersize distribution plots of Au-PEI@NIST measured by TEM. Bin widths are 1.0 nm.

TEM is a 'dry' method to visualize and measure the hard-core size and shape of targeted particles. On the other hand, DLS is a 'wet' method for size determination, and it provides a spherical-equivalent hydrodynamic size of the total particle entity. Hydrodynamic size is typically larger than hard-core size for a given particle. This is, in fact, what we find in our analysis of Au-PEI@NIST.

5.1.3. Particle height by AFM

Incubate a mica substrate with a drop of 0.1% poly-L-lysine (PLL) for several minutes, then rinse it with DI water and blow dry with compressed air supplied by an AML fume hood.[§]

Immediately after drying, incubate the PLL-functionalized mica substrate with a drop of the as-prepared Au-PEI@NIST solution for 1 hour, before rinsing in DI water to remove unattached particles. Blow dry deposited substrate gently with compressed air (or nitrogen). Representative AFM images are obtained with a described AFM system (Sec. 3.2). Nanoscope Version 6 software is used for data acquisition. Imaging is performed in a tapping mode using Veeco OTESP cantilevers. Calibration of the height, or Z axis of the AFM should be performed using a step height reference standard commensurate with the size of Au-PEI@NIST (e.g., a 7-nm NANO2 step height reference standard is used to obtain representative results in Figure 3). AFM images of individual particles are analyzed using routines provided with the Nanoscope Version 5 image analysis software. A first-order image flattening routine is applied to correct global background tilt to obtain particle height measurements. Particles are excluded from each image before fitting the background tilt. To obtain a statistically meaningful estimate

---

[§] Note that the Au-PEI@NIST nanoparticles are cationic, hence expected to attach to negatively charged surfaces. However, on freshly cleaved mica, which has a highly negative surface charge, the coverage density of particles was surprisingly low after a 1-hour incubation of the as-received full-strength solution. To improve the surface attachment of the Au-PEI@NIST nanoparticles, the mica was treated with an expired poly-L-lysine (PLL) solution. The use of an expired PLL solution (several years past stated expiration date) was found to be more efficient than a newer (not expired) solution for depositing sufficient particles for AFM imaging. This is a critical procedure step although the reason for this is not well understood.

This publication is available free of charge from: https://doi.org/10.6028/NIST.SP.1200-29

of the particle size distribution, more than 1300 individual nanoparticles are measured from multiple locations across the sample. The histogram of measured relative quantities and the cumulative height distribution obtained by AFM are shown in Fig. 3 along with a representative AFM topography image. The height, which represents the core size of Au-PEI@NIST, ranges from 4 nm to 15 nm with a mean height and standard deviation of (10.4 ± 1.7) nm. The median height (d_{50}) value as determined from the cumulative distribution is 10.8 nm. The results by AFM and TEM agree within the uncertainty bound of one standard deviation of the respective measurements.
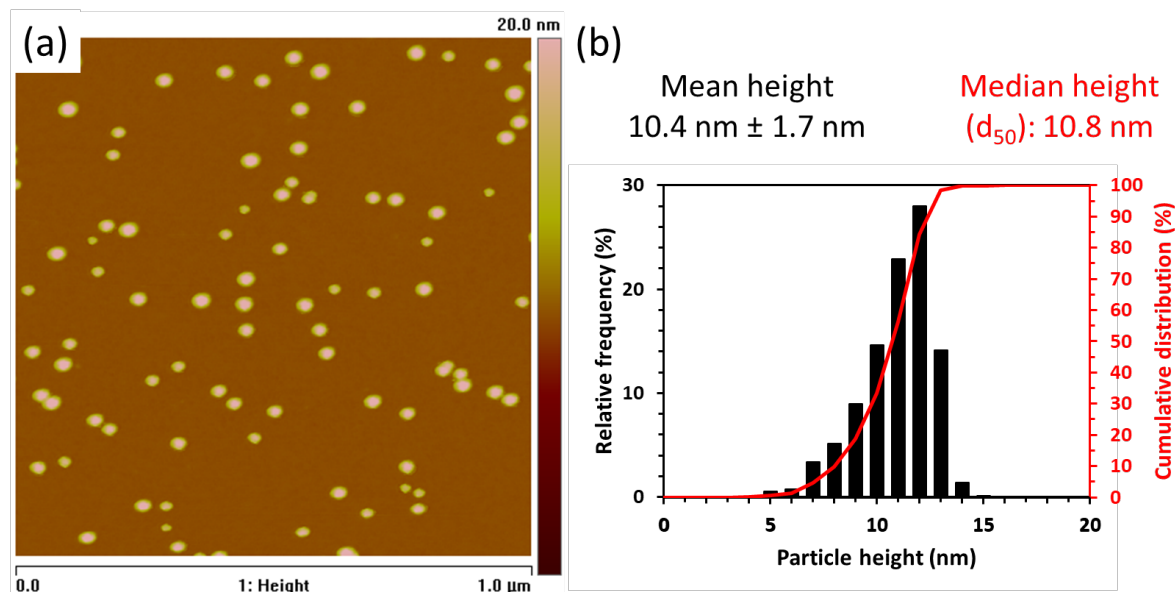
Fig. 3. (a) Representative AFM image of the Au-PEI@NIST. (b) Histogram of relative quantities and cumulative height distribution of Au-PEI@NIST measured by AFM. Bin widths are 1.0 nm.

5.2. Optical properties

Sample preparation for UV-Vis analysis is identical to that for DLS measurement, and in fact the same cuvette/sample can be used if the cuvette is compatible with both instruments and is UV transparent. The maximum absorption (λ_{max}) of the surface plasmon resonance (SPR) band for Au-PEI@NIST occurs at 521 nm for the product produced in this study (Figure 4); this value is typical for this size range of spheroidal AuNPs. Small shifts of 1 nm to 2 nm can be expected from batch to batch. The narrowness (or broadness) of this band reflects the narrowness (or broadness) of the core size and the consistency or variability of the particle shape.
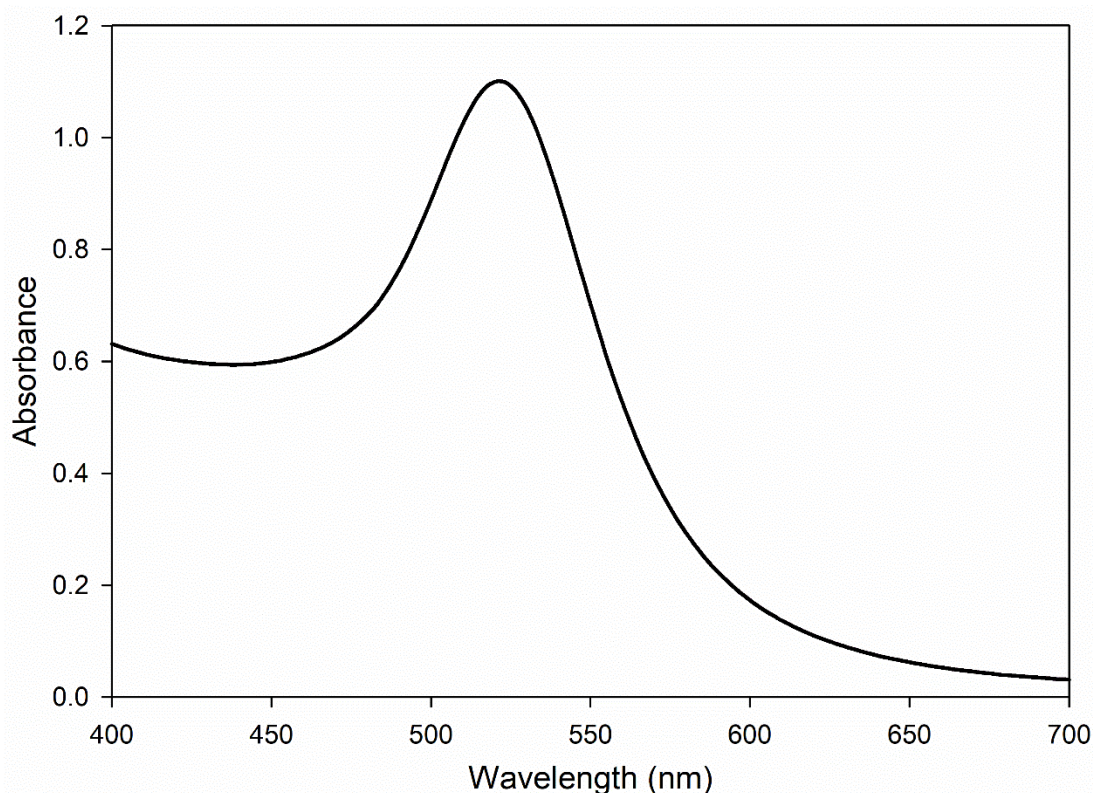
Fig. 4. Representative UV-Vis absorption spectra for Au-PEI@NIST in DI water ($f = 10$), showing the strong SPR peak at 521 nm.

5.3.   Surface charge (Zeta potential)

Sample preparation for zeta potential analysis is identical to that for DLS (≈ 50 mg/L; diluted in DI water, $f = 10$, pH ≈ 9). Zeta potential reflects the surface charge properties of the suspended particles in a particular medium (i.e., it is a system property, not a particle property). Representative zeta potential results for Au-PEI@NIST were obtained using a palladium dip cell and a Malvern Panalytical Zetasizer Nano instrument. The mean zeta potential measured was ($+15.6 \pm 0.9$) mV, which reflects the cationic surface resulting from the PEI corona.

5.4.   Surface coverage (mass ratio of PEI to Au) by TGA

To prepare a sample for TGA analysis, 20 mL of stock solution is first concentrated by rotary evaporation at a temperature of 60 °C, until the remaining amount is 200 µL to 300 µL. Then 5 µL of the concentrated product is directly cast into an alumina crucible and dried on a hotplate at 70 °C for 15 min. Repeat this procedure 5 to 10 times until the weight of dried-accumulated sample in the crucible is reached to 8 mg to 10 mg. After which, the crucible is transferred into a vacuum-desiccator for further drying overnight. Careful drying and slow initial heating rates are important for these samples to avoid bursting/splashing due to excess retained water (see below for more details). In the present case, the mass ratio of PEI to Au is evaluated using TGA and freshly prepared Au-PEI@NIST as described below.

Two separate TGA measurements are performed on each sample – the sample temperature is first ramped up to 600 °C for measurement in ultra-high purity (UHP) argon, then again in UHP air (mixture of 80 % UHP nitrogen and 20 % UHP oxygen) heated to 900 °C to ensure full removal of carbon moieties. Three replicate samples are measured, and the results are

9

shown in Figure 5. For the initial TGA cycle in argon, the sample is first heated to 100 °C at 10 °C/min rate, then to 150 °C at 1 °C/min and held at 150 °C for 3 hours to remove all chemisorbed water, then to 600 °C at 10 °C/min for the decomposition of PEI, followed by cooling to room temperature. We have confirmed the validity of the step for removing residual water by evaluating mass loss while holding pure PEI (no gold) at 150 °C in UHP argon for 3 hours as a control experiment. The sample is then ramped to 900 °C in UHP air at 10 °C/min to remove any organic residuals from the decomposition of PEI during the TGA in UHP argon. As a result, the mass ratio of PEI to Au in the Au-PEI@NIST is determined with one standard deviation as 5.60 ± 0.24. This value demonstrates that about 28 % of initially applied PEI mass is conjugated after the reduction of Au^{III} (see Sec. 4.1). Additionally, as shown in Fig. 5, there is significant water retained in the sample, evidenced by the mass loss (approximate 26.8 %) while heating to 150 °C and subsequent holding at 150 °C in UHP argon. The PEI losses from the decompositions in UHP argon and UHP air are approximately 56 % and 6.6 %, respectively, and the mass residual is approximately 10.7 %, representing the mass fraction of gold in the sample.
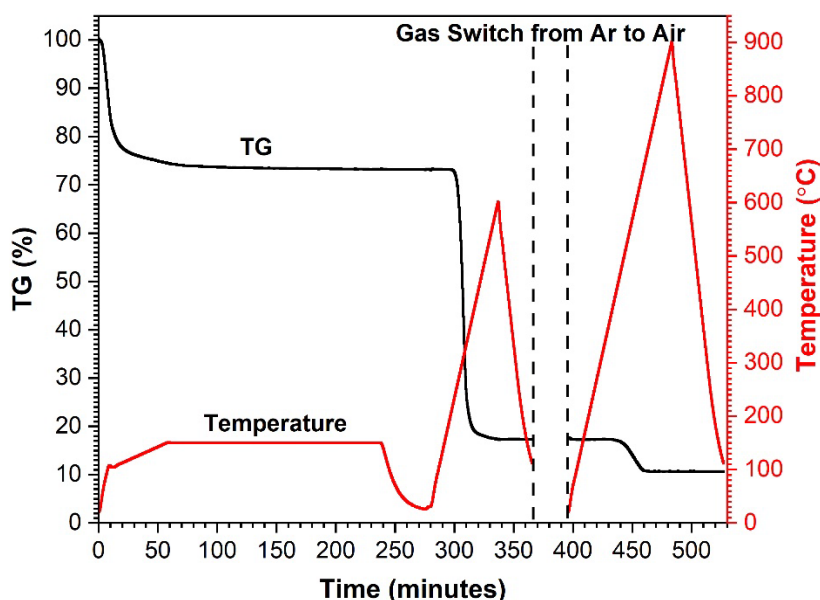
Fig. 5. Representative TGA results for Au-PEI@NIST merged from two separate measurements, with the first measurement in UHP argon and the second measurement in UHP air (mixture of 80 % UHP nitrogen and 20 % UHP oxygen).

6. Assessing colloidal stability

General sample preparation(25):
Stability assessment of AuNP@NIST in shelf-life, media, and various pHs are conducted after dilution into the selected medium (DI water for shelf-life test; dilution factor (*f*) = 10). The final recommended concentrations of AuNPs in test aliquots are in the range of (5 to 50) mg/L (or ppm) for both DLS and UV-Vis measurements. The pH is adjusted using 0.05 mol/L HCl (aq.) and/or 0.05 mol/L NaOH (aq.) solution. The test of lyophilization-reconstitution cycle is conducted without further dilution of the stock suspension.

10

6.1. Shelf-life

Long term shelf-life (e.g., 1 to 3 years) is typically assessed by storing the stock suspension under ambient laboratory conditions (typically from 20 °C to 25 °C and away from direct light) and repeating the measurements after the long term storage. This is only possible if the suspension has been handled under sterile conditions (e.g., filtered and transferred inside a biological safety cabinet using sterile procedures). The freshly prepared Au-PEI@NIST is first analyzed by DLS and UV-Vis (Figure 6) for later comparison. Then samples are drawn and prepared for DLS and UV-Vis analysis at appropriate times (maintaining sterile conditions while doing so). Analyses of Au-PEI@NIST before and after the long-term storage for 3 years are compared in Fig. 6 for its size and optical absorbance measurement results. The mean hydrodynamic size and SPR maximum wavelength are nearly unchanged after 3 years: (23.7 ± 0.3) nm versus (24.2 ± 0.2) nm and 521 nm versus 520 nm, for the stored and freshly prepared samples, respectively. This demonstrates that Au-PEI@NIST is exceptionally stable under ambient conditions. Furthermore, the zeta potential for the aged material still shows a positive surface charge of (19.6 ± 0.9) mV, indicating notable long-term stability of the PEI surface coating on Au-PEI@NIST.
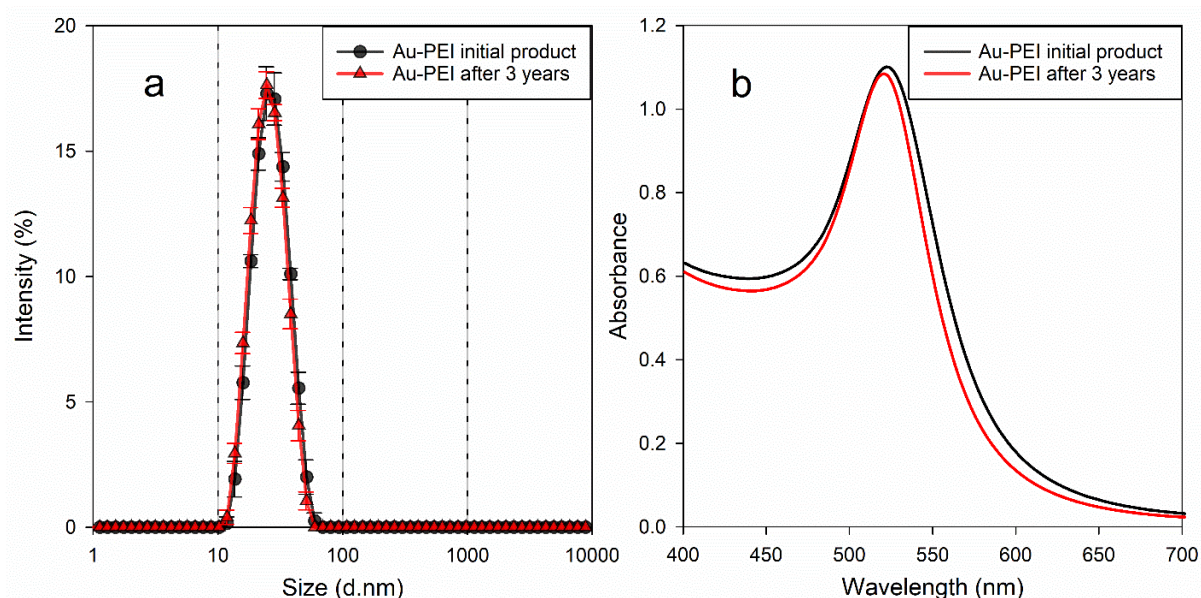
Fig. 6. Representative data showing long term stability ("shelf-life") of Au-PEI@NIST examined by DLS (a) and UV-Vis (b) in DI water ($f = 10$). Black line: initially purified samples; red line: after 3 years.

6.2. Stability in physiological media

The evaluation of colloidal stability in physiological (isotonic) media is conducted by dilution ($f = 10$) of Au-PEI@NIST into PBS, M9 buffer and/or DMEM (or other relevant media, such as plasma). Samples are prepared as above for UV-Vis analysis, and UV-Vis absorbance is monitored over the time period up to 72 h at 20 °C.(25)

In Figure 7a and 7b, representative data for Au-PEI@NIST shows exceptional stability in PBS and M9 buffer, respectively. The SPR band, with respect to absorbance intensity and wavelength, exhibit virtually no change over 72 h. PBS and M9 buffer are composed mostly of salts and have sufficient ionic strength to produce a strong charge screening effect capable of agglomerating charge-stabilized particles. Clearly, Au-PEI@NIST tolerates charge

11

screening and affords consistent stability in saline media up to at least 3 days. DMEM, a common cell culture medium that includes (in addition to salts) amino acids, vitamins, glycine, serine and ferric nitrate, is a more complex medium. Au-PEI@NIST exhibits significant change in UV-Vis spectra over 72 h in DMEM (Fig. 7c), with a decrease in the SPR maximum intensity of $\approx$ 18 % at 520 nm and a slight red-shift ($\Delta\lambda_{max}$ = 2 nm, over 72 h) in the maximum wavelength. From these results we conclude that one or more of the non-salt components interacts sufficiently with particles to induce a measurable but still fairly moderate level of agglomeration.(23)

An additional stability test in [DMEM +10 % BSA] (Fig. 7d) shows that, in the presence of a moderate concentration of serum protein, stability is substantially recovered. Here the SPR band absorbance is reduced by $\approx$ 8 % with red-shift ($\Delta\lambda_{max}$ = 2 nm) over the first 6 h, differently from in DMEM only (no red-shift observed over 24 h). The early observed red-shift could be attributed to conjugation of Au-PEI@NIST with BSA, however in spite of this initial intensity loss and red-shift of the SPR band, there is no further conformational change or morphological transformation apparent with Au-PEI@NIST up to 72 h (i.e., there is an initial moderate effect, but otherwise the complex is colloidally stable for long periods of time in DMEM+BSA). Size analysis can make this characteristic colloidal behavior in physiological media more convincing. Notably, the DLS measurements (insets in Fig. 7) exhibit very consistent z-average sizes in both PBS and M9 buffer (Fig. 7a, b) over time, which indicates remarkable colloidal stability. However, DLS reveals significant changes of z-average size during the same period (over 72 h) in DMEM (Fig. 7c). Although the z-average size in this case is not reliable on numerical accuracy due to multimodal size distributions, the trend of size change over time implies that the agglomeration measurably occurs till 36 h and following sedimentation afterwards without further significant agglomeration. Histograms of size distributions in DMEM (Figure 7e) are affirmative. Compared to the initial measurement (at 0 h, black circle in Fig. 7e) of the sample in DMEM, the size distribution of the sample aged 36 h (red square) shows a markedly decreased intensity at $\approx$ 25 nm along with a newly appeared peak (at $\approx$ 450 nm). After 72 h, histogram exhibits (blue triangle) the comeback of the peak intensity at 25 nm and reduced intensity of agglomerates in larger size range. In [DMEM +10 % BSA], analysis of the 'z-average size versus time' is not successful due to the dominant interfering peaks by BSA intervening (plot of size versus time is omitted; no inset in Fig. 7d). However, DLS measurement exhibits the size-shift of AuNPs from $\approx$ 25 nm (in other media) to $\approx$ 60 nm (broadened) due to conjugation with BSA, which agrees to the slight early red-shift of SPR by UV-Vis (Fig. 7d). In addition, in Fig. 7f, DLS histogram of medium only at 0 h exhibits a peak at $\approx$ 6 $\sim$ 7 nm (monomeric BSA; black circle), and after 72 h, it shows an additional peak at $\approx$ (70 to 400) nm for x-meric BSA over time (green triangle). On the other hand, the conjugation between Au-PEI@NIST and BSA is observed in identical medium at the initial state (red square). Based on the broadening and overlapping peak of bigger size range (yellow diamond), that conjugation still exists after 72 h along with the new occurrence of x-meric BSA components and presumably slight agglomeration. The results suggest that the Au-PEI@NIST in [DMEM +10 % BSA] interacts with BSA initially due to the much higher concentration of BSA in medium rather than the agglomerates between Au-PEI@NIST particles, then keeps conjugation status mostly with perhaps minor agglomeration over time. These DLS analyses can further support the less consistent behaviors than those in salty media that we expected from the observation by UV-Vis. Overall, the results obtained from UV-Vis and DLS studies on colloidal stabilities in physiologically relevant media agree well with each other.
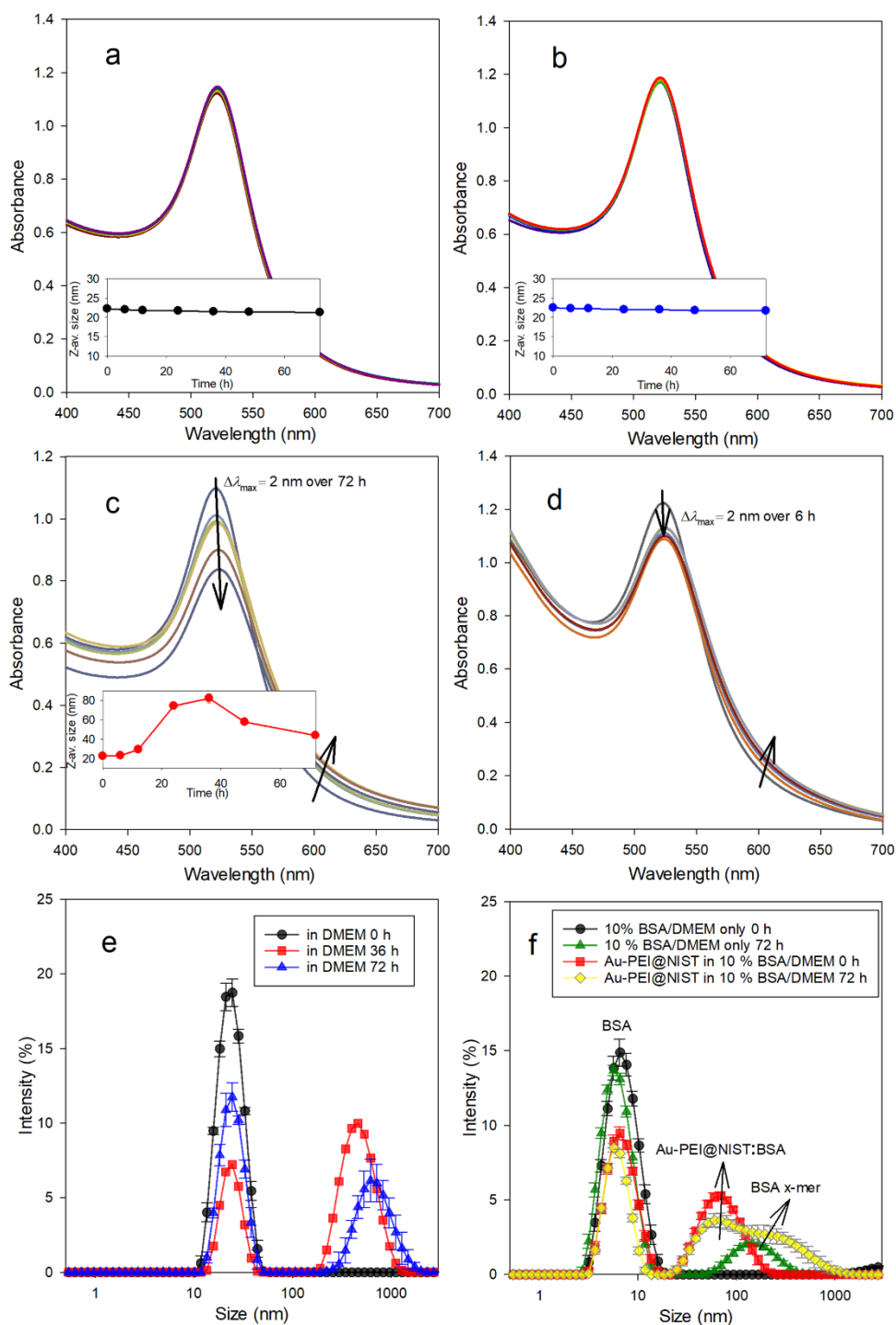
Fig. 7. Representative data showing the colloidal stability of Au-PEI@NIST over 72 h at 20 °C evaluated in physiological media (f = 10): by UV-Vis (a) PBS, (b) M9 buffer, (c) DMEM, (d) DMEM containing 10 % BSA. Insets in panels (a, b, and c) are plots of z-average size versus time and arrows (in c and d) show the direction of change; by DLS (e) size distributions over time in DMEM and (f) DMEM containing 10 % BSA. Arrows in panel e are simply indicating components in test sample.

13

6.3.   pH dependency

To assess the pH-dependent stability of Au-PEI@NIST, samples were prepared in the same manner as for DLS and UV-Vis, but with pH-adjusted solutions used for dilution ($f = 10$). Representative data in Figure 8 shows mostly overlapped SPR curves in all panels, indicating excellent stability over a wide pH range from highly acidic (Fig. 8a, pH < 2) to highly alkaline (Fig. 8c, pH > 12) over 12 h at 20 °C.
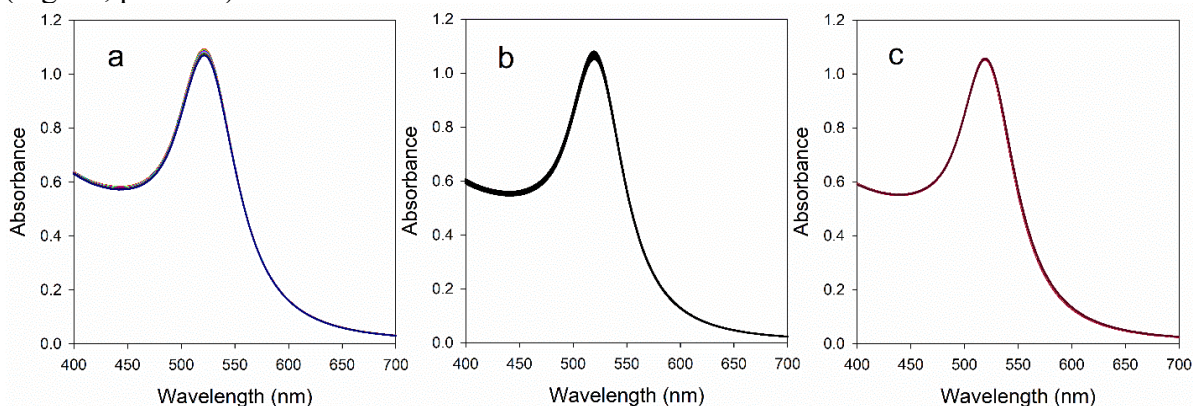
Fig. 8. Representative pH-dependent stability data for Au-PEI@NIST; (a) 50 mmol/L HCl, (b) pH 7.2, and (c) 50 mmol/L NaOH over 12 h at 20 °C.

6.4.   Thermal stability

The thermal stability for Au-PEI@NIST is monitored by UV−Vis over the range from (20 to 70) °C, which covers the relevant range for most biomedical applications. As the temperature is increased stepwise, the sample (diluted in DI water, $f = 10$) is incubated for 30 min at each temperature to conduct measurement at an equilibrated temperature. Representative data (Figure 9) show that Au-PEI@NIST is thermal stability over the tested range based upon the invariance of the SPR band (from UV−Vis spectra).
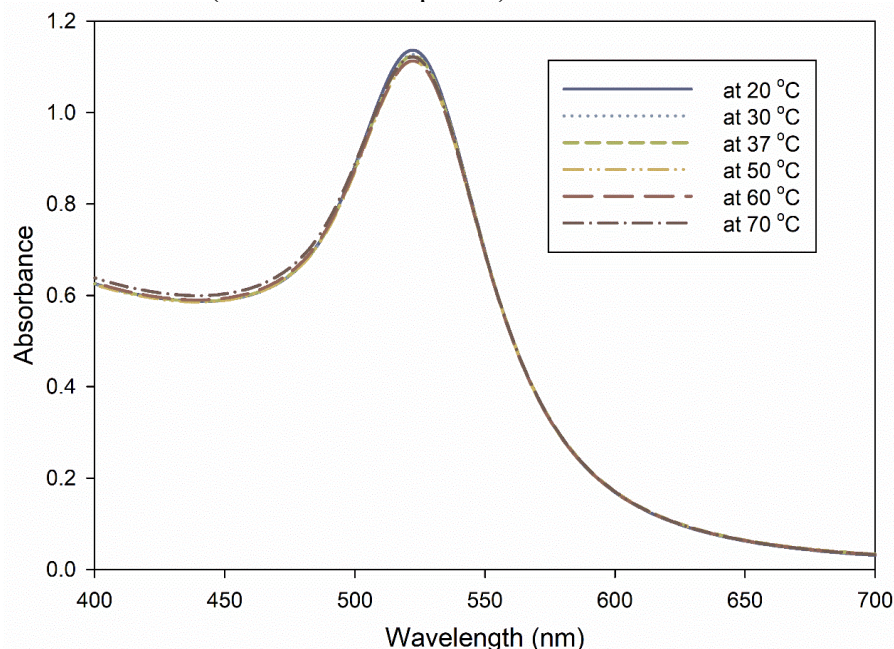
Fig. 9. Representative thermal stability data for Au-PEI@NIST evaluated by UV-Vis. Sample was incubated for 30 min at each temperature prior to measurement.

14

6.5. Lyophilization-reconstitution cycle

As a potential alternative approach to the long-term stability test, we assessed the response of Au-PEI@NIST to a lyophilization-reconstitution cycle.(29) In general, place a known volume of stock suspension into an appropriate lyophilization vial and rapidly freeze the solution by dipping the vial into liquid nitrogen in a Dewar. The frozen test material is then placed into a freeze-drier and lyophilized until all moisture is removed. After lyophilization, reconstitute the dried Au-PEI@NIST by adding the same known volume of DI water, mixing moderately, then store overnight at ambient temperature and measure DLS and UV-Vis to compare before and after one cycle. The whole cycle is processed without the aid of excipients. The visual status of Au-PEI@NIST at each step of the lyophilization-reconstitution cycle is displayed in Figure 10. The color and translucence of suspensions before and after lyophilization-reconstitution are visually similar, which suggests that Au-PEI@NIST is relatively tolerant of this process. However, further characterization provides more detail and insight.

Fig. 10. Visual observation of Au-PEI@NIST at each step of lyophilization-reconstitution cycle; (left) original suspension (before cycle), (middle) lyophilized material, and (right) reconstituted suspension after full cycle (resuspended in DI water). The reconstituted material shows similar characteristic translucent red color implying stable unaggregated AuNPs in this size range.

In Figure 11a, a UV-Vis spectrum for reconstituted material after the lyophilization-reconstitution cycle (red triangles) shows a slightly red-shifted ($\Delta\lambda_{max} \approx 2$ nm) SPR band with significantly decreased intensity (≈ 20 %, at 523 nm) and with increased and broadened absorbance at higher wavelengths. The DLS size distribution of the post-cycle material (Fig. 11b, red triangles) exhibits a substantial increase in the mean z-average size ($\Delta d_z \approx 40$ nm) and broadening of the distribution, despite a relatively small change in the SPR peak band (minimal red shift) and a visual similarity.

Notably, the pre-cycle size distribution is recovered by simply incubating the reconstituted suspension at 70 °C for 2 h. The green squares in Fig. 11a and 11b are the results from the post-incubation reconstituted suspension, leading to the following summary. First, there is no substantial change in the UV-Vis absorbance spectrum compared to the pre-incubation reconstituted sample. On the other hand, the hydrodynamic size distribution after incubation

has decreased substantially and now virtually overlays the pre-incubation results ($\Delta d_z \approx 1.5$ nm).

A plausible explanation for this observed behavior is that the PEI shell prevents gold cores from contacting during the freezing step, despite the obvious formation of Au-PEI@NIST agglomerates. These agglomerates are largely separable into individual particles due to the non-interacting gold cores. The application of heat (thermal energy) is sufficient to separate flocculated material into singlet particle complexes. These preliminary results demonstrate a potential methodology for very long term storage under almost any condition, which would simplify transport and greatly increase shelf-life. Further work would be needed to optimize this process.
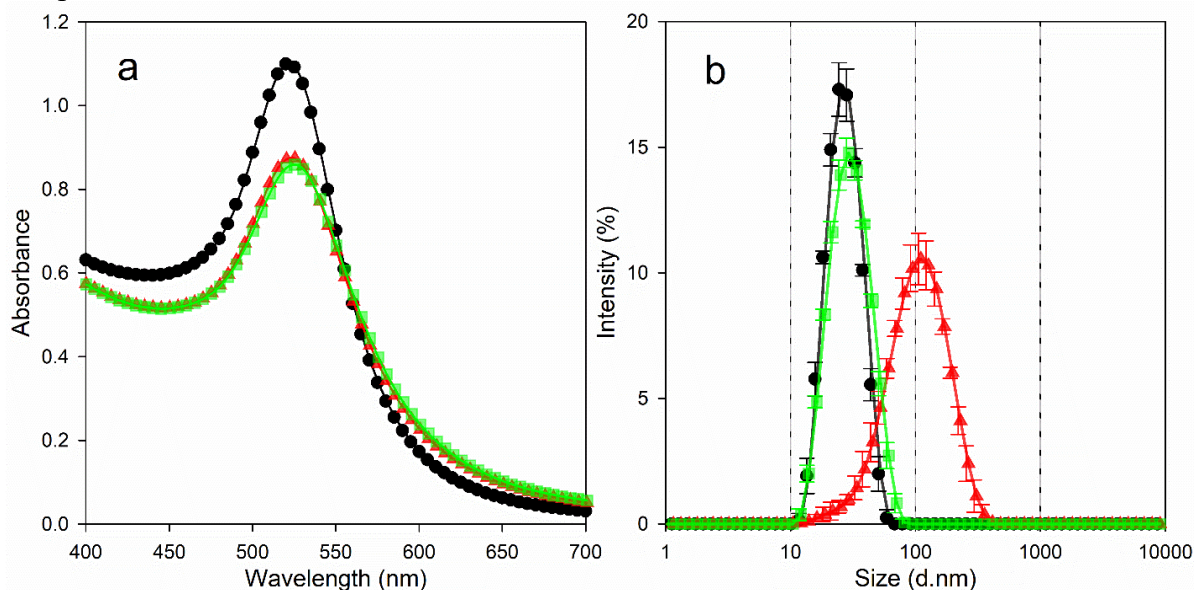
Fig. 11. Comparison of (a) UV-Vis absorbance spectra and (b) DLS intensity-weighted size distributions for Au-PEI@NIST before (black dots) and right after (red triangles, without thermal incubation) a lyophilization-reconstitution cycle. Green squares in both panels (SPR and size in a and b, respectively) represent recovery behaviors of reconstituted material after thermal incubation.

7. Reproducibility

As a quality check of the consistent synthetic, reproducibility is monitored for a series of 100 mL material from different batch syntheses. As shown in Table 1, this synthetic procedure yields excellent reproducibility with the support of consistent size, optical properties, and surface charge. An average hydrodynamic size of (23.7 ± 0.4) nm with a coefficient of variation of 1.7 % and optical absorbance spectra (Figure 12) with SPR maximum (λ_{max}) consistently at 522 nm are observed. The peak maximum optical density (at 522 nm) has a coefficient of variation of 2.4 %.

Table 1. Reproducibility of Au-PEI@NIST small-batch synthesis, showing mean hydrodynamic size and polydispersity index, SPR band peak and optical density, and zeta potential for each batch and means for all batches. Uncertainties represents one standard deviation of 5 replicate measurements of one Au-PEI sample from each batch.

16

Au-PEI@NIST Batch #	d_Z^a (nm)/PdI^b	SPR^c λ_{max} (nm)/optical density	Zeta Potential^d (mV)
1	23.6 ± 0.3/*0.12*	522/1.076	+ 33.9 ± 0.9
2	24.1 ± 0.1/*0.11*	522/1.025	+ 34.4 ± 0.8
3	23.3 ± 0.2/*0.12*	522/1.052	+ 36.4 ± 0.7
Average	23.7 ± 0.4 /*0.12*	522/1.051	+ 34.9 ± 1.3

[a]hydrodynamic (z-average) size obtained by DLS, [b]polydispersity index, and [c]surface plasmon resonance band by UV-Vis measurements, and [d]zeta potential by DLS.
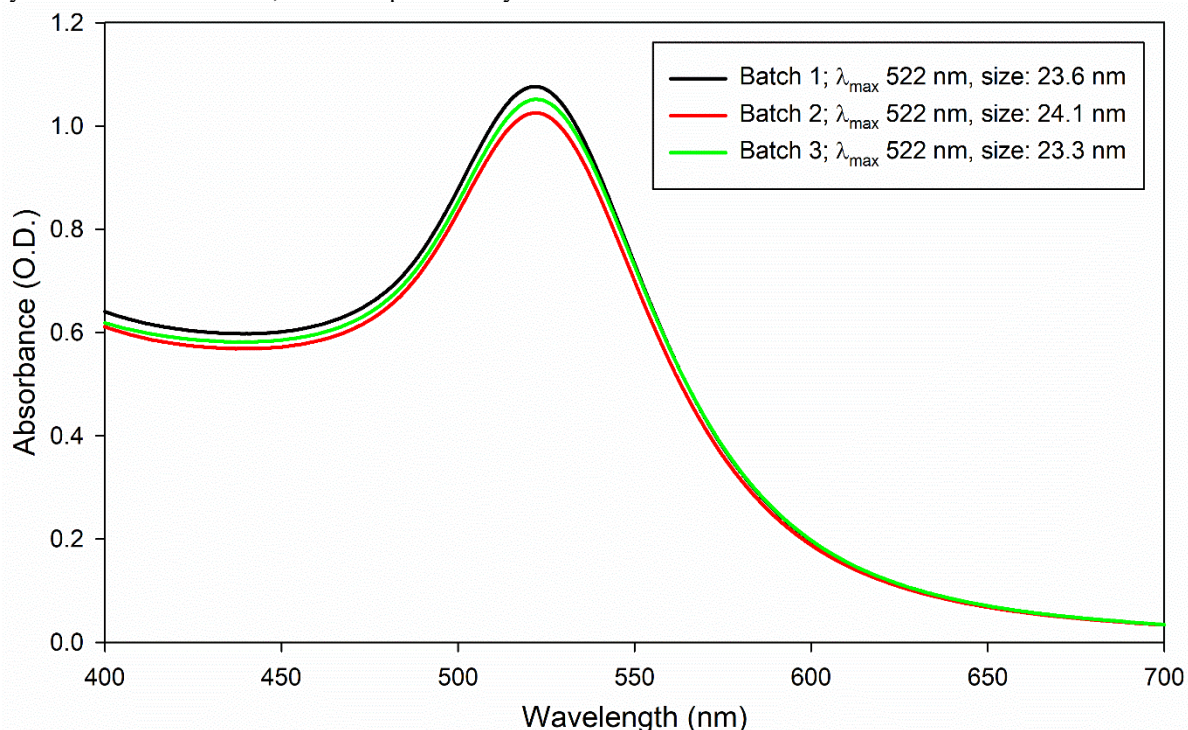

Fig. 12. Reproducibility of Au-PEI@NIST prepared using the optimized condition in 100 mL scale reactions; UV-Vis absorbance spectra are shown. The inset lists the values of λ_{max} and the average z-average (hydrodynamic) diameter for each replicate reaction.

8. Cytotoxicity

Cytotoxic effect of Au-PEI@NIST was evaluated for Chinese hamster ovary (CHO) K1 cells using the MTS (3-(4,5-dimethylthiazol-2-yl)-5-(3-carboxymethoxyphenyl)-2-(4-sulfophenyl)-2H-tetrazolium)\PMS(phenazine methosulfate) cell viability assay. The MTS assay is a screening assay and provides a rapid method to assess potential toxic interactions with biological cells. The reagent is reduced in the presence of cellular enzymes and forms a colored product that is soluble in the culture media. The optical density of the culture media measured at 490 nm is correlated with cell count in the culture conditions. Stock cultures of CHO K1 cells (ATCC, Manassas, VA, USA) were grown for 24 h at 37 °C, 5 % CO_2 and 95 % relative humidity in Iscove's modified Dulbecco's modified medium, IMDM (Gibco, Carlsbad, CA), 10 % (v/v) fetal bovine serum (FBS, Gibco), 1% (v/v) penicillin-streptomycin (100 units/mL, and 100 µg/mL). Measurement procedure was adopted from ISO 19007:2018 (Nanotechnologies−*In vitro* MTS assay for measuring the cytotoxic effect of nanoparticles; www.iso.org/standard/63698). Briefly, on day 1, a 96-well plate is seeded with 12,500

17

cells/well and incubated for 24 h. On day 2, the supernatant is decanted, cells are rinsed with warm PBS and a series dilution of Au-PEI@NIST concentrations in the media are loaded in three replicates along with a negative control (media only), positive control – cadmium sulfate ($CdSO_4$), and cationic cerium oxide nanoparticle (CeO_2 NP) suspension for comparison purposes. One column is left with no cells to account for nanoparticle optical interference. Following a 24 h incubation, the test solutions are decanted, the plate is rinsed with PBS and filled with 100 µL of MTS reagent. After 1 h incubation at 37 °C, 5 % CO_2 and 95 % relative humidity, the absorbance is recorded at 490 nm. The average background level for nanoparticles in the culture medium is subtracted for each well. The resulting absorbance from each well is then normalized to the absorbance value from the well with no nanoparticles. In that way, background subtracted, and normalized values represent the fraction of cells that remain after Au-PEI@NIST, and CeO_2 NP dose treatment (Figure 13).
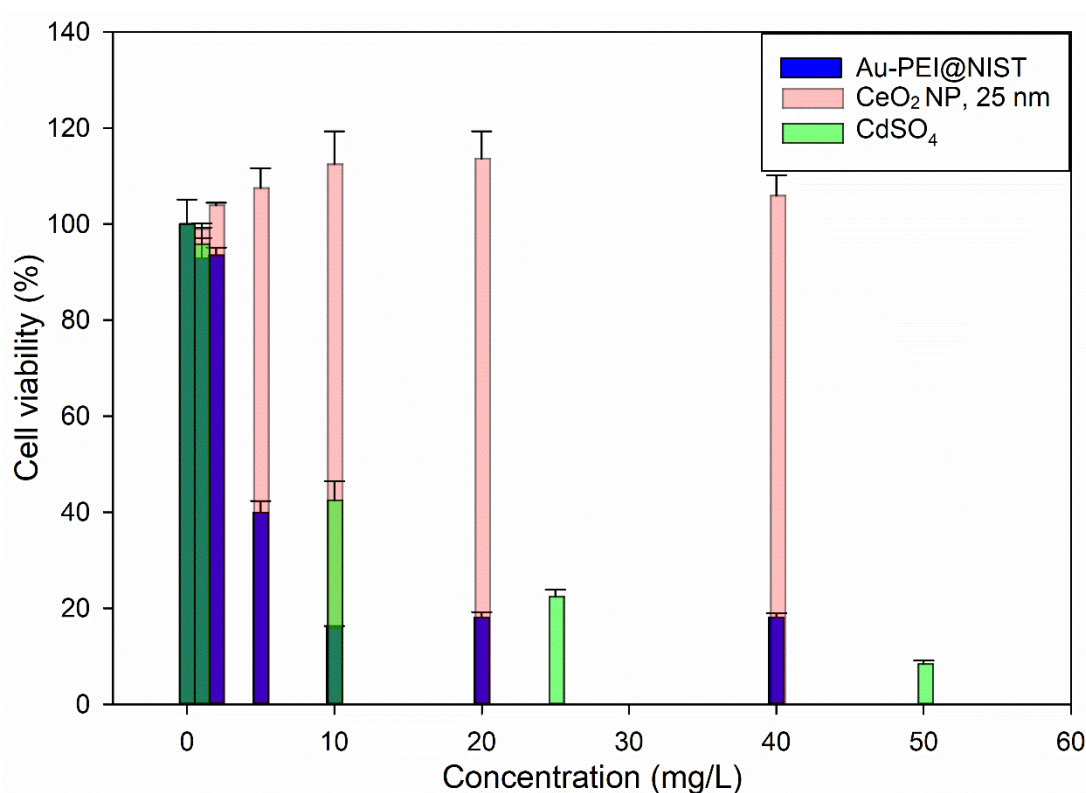
Fig. 13. MTS cell viability assay results for CHO K1 cell line after 24 h exposure to Au-PEI@NIST nanoparticles (blue), CeO_2 NP (red), and $CdSO_4$ (green, as a positive control).

Cell viability is calculated as follows: viability (%) = [(Experimental A_{490nm} - Background A_{490nm})/(Negative control A_{490nm} - Background A_{490nm})] x 100. The data are expressed as means ± standard deviation from three separate measurements. Representative data in Figure 13 shows that Au-PEI@NIST decreases CHO cell viability in a dose dependent manner. A dose lethal to 50 % of cells following 24 h estimate $LD_{50} = (1.96 \pm 0.15)$ µg/mL (in Fig. 13, blue bars) was obtained by approximating the viability data to a continuous concentration-response curve by a non-linear fit. Highly cationic CeO_2 NPs (d < 25 nm, average zeta potential in the growth media ((150.7 ± 21.4) mV)) did not exhibit toxicity to CHO cells at concentrations up to 40 µg/mL (red bars, Fig. 13). Cell viability values higher than 100% resulted likely resulted

from the hormesis effects.(30) Particle toxicity of Au-PEI@NIST to tested mammalian cells (CHO K1) is significantly higher compared to the cationic CeO_2 NP or even $CdSO_4$, the positive control (green bars, $LD_{50} = (24 \pm 4.2)$ µg/mL).

9. Summary

This study demonstrates the preparation of 100 mL scale of Au-PEIs using 10 % (mass fraction) of branched PEI (25 kDa) and 2.5 mmol/L of $HAuCl_4$ at a molar ratio ($r^{PEI/Au}$) = 96 and a temperature ramping program of (r.t. to 80) °C for 3 h (after reaching the desired temperature) results in highly quality of Au-PEI@NIST in terms of narrowness in size distribution and optical property (SPR), long term colloidal stability, and stable behaviors in physiologically relevant conditions. In addition to stability and a narrow size distribution, Au-PEI@NIST exhibits shape uniformity (by TEM and AFM) and positive surface charge (by zeta potential). Moreover, this optimized template for Au-PEI synthesis shows high reproducibility confirmed by monitoring hydrodynamic diameter and SPR. The surface coverage of PEI on the gold core as a mass ratio is characterized by TGA measurement. The cytotoxicity of Au-PEI@NIST on CHO-K1 cells is significantly higher than that of the positive control ($CdSO_4$). Thus, this toxicity result reveals the potential of usage of Au-PEI@NIST as a nano-scale positive control in the fields of nanotoxicology and nanomedicine.

10. Acronyms/Abbreviations

aq	aqueous
AFM	atomic force microscope
AML	advanced manufacturing laboratory
AuNP(s)	gold nanoparticle(s)
Au-PEI	PEI conjugated gold nanoparticles
BSA	bovine serum albumin
CHO	chinese hamster ovary
DI	deionized
DLS	dynamic light scattering
DMEM	Dulbecco's modified eagle medium
FBS	fetal bovine serum
IMDM	Iscove's modified Dulbecco's modified medium
MTS	3-(4,5-dimethylthiazol-2-yl)-5-(3-carboxymethoxyphenyl)-2-(4-sulfophenyl)-2H-tetrazolium
NCL	Nanotechnology Characterization Laboratory
NIST	National Institute of Standards and Technology
PBS	phosphate buffer saline
PdI	polydispersity index
PEI	polyethyleneimine
PMMA	polymethylmethacrylate
PMS	phenazine methosulfate
ppm	part per million
SPR	surface plasmon resonance
TEM	transmission electron microscope
TGA	thermogravimetric analysis

UHP   ultra-high purity
UV-Vis   ultraviolet-visible

11. References

[1]   National Nanotechnology Initiative (NNI) (2011) Environmental, Health, and Safety Research Strategy; Presidents Council of Advisors on Science and Technology: National Science and Technology Council Committee on Technology, Washington, DC.

[2]   Giljohann DA, Seferos DS, Daniel, WL, Massich MD, Patel PC, Mirkin CA (2010) Gold Nanoparticles for Biology and Medicine. *Angewandte Chemie-International Edition 49*(19):3280−3294. https://doi.org/10.1002/anie.200904359

[3]   Shukla R, Bansal V, Chaudhary M, Basu A, Bhonde RR, Sastry M (2005) Biocompatibility of gold nanoparticles and their endocytotic fate inside the cellular compartment: A microscopic overview. *Langmuir 21*(23):10644−10654. https://doi.org/10.1021/la0513712

[4]   Cho EC, Xie JW, Wurm PA, Xia YN (2009) Understanding the Role of Surface Charges in Cellular Adsorption versus Internalization by Selectively Removing Gold Nanoparticles on the Cell Surface with a I-2/KI Etchant. *Nano Letters 9*(3):1080−1084. https://doi.org/10.1021/nl803487r

[5]   Taylor U, Klein S, Petersen S, Kues W, Barcikowski S, Rath D (2010) Nonendosomal Cellular Uptake of Ligand-Free, Positively Charged Gold Nanoparticles. *Cytometry Part A 77A*(5):439−446. https://doi.org/10.1002/cyto.a.20846

[6]   Arvizo RR, Miranda OR, Thompson MA, Pabelick CM, Bhattacharya R, Robertson JD, Rotello VM, Prakash YS, Mukherjee P (2010) Effect of Nanoparticle Surface Charge at the Plasma Membrane and Beyond. *Nano Lett 10*(7):2543−2548. https://doi.org/10.1021/nl101140t

[7]   Lee SH, Bae KH, Kim SH, Lee KR, Park TG (2008) Amine-functionalized gold nanoparticles as non-cytotoxic and efficient intracellular siRNA delivery carriers. *International Journal of Pharmaceutics 364*(1):94−101. https://doi.org/10.1016/j.ijpharm.2008.07.027

[8]   Niidome T, Nakashima K, Takahashi H, Niidome Y (2004) Preparation of primary amine-modified gold nanoparticles and their transfection ability into cultivated cells. *Chemical Communications* (17):1978-1979. https://doi.org/10.1039/b406189f

[9]   Noh SM, Kim WK, Kim SJ, Kim JM, Baek KH, Oh YK (2007) Enhanced cellular delivery and transfection efficiency of plasmid DNA using positively charged biocompatible colloidal gold nanoparticles. *Biochimica et Biophysica Acta-General Subjects 1770*(5):747−752. https://doi.org/10.1016/j.bbagen.2007.01.012

[10] Sandhu KK, McIntosh CM, Simard JM, Smith SW, Rotello VM (2002) Gold nanoparticle-mediated Transfection of mammalian cells. *Bioconjugate Chemistry 13* (1):3−6. https://doi.org/10.1021/bc015545c

[11] Song WJ, Du JZ, Sun TM, Zhang PZ, Wang J (2010) Gold Nanoparticles Capped with Polyethyleneimine for Enhanced siRNA Delivery. *Small 6*(2):239−246. https://doi.org/10.1002/smll.200901513

[12] Thomas M, Klibanov AM (2003) Conjugation to gold nanoparticles enhances polyethylenimine's transfer of plasmid DNA into mammalian cells. *Proceedings of the*

National Academy of Sciences of the United States of America 100(16):9138−9143. https://doi.org/10.1073/pnas.1233634100

[13] Ghosh PS, Kim CK, Han G, Forbes NS, Rotello VM (2008) Efficient Gene Delivery Vectors by Tuning the Surface Charge Density of Amino Acid-Functionalized Gold Nanoparticles. *Acs Nano 2*(11):2213−2218. https://doi.org/10.1021/nn800507t

[14] Bekturov EA, Mamutbekov GK (1997) Syntheses and properties of films from polymer gels based on polymer-metal complexes. *Macromolecular Chemistry and Physics 198*(1):81−88. https://doi.org/10.1002/macp.1997.021980107

[15] Kramer G, Buchhammer HM, Lunkwitz K (1998) Investigation of the stability of surface modification by polyelectrolyte complexes - influence of polyelectrolyte complex components and of substrates and media. *Colloids and Surfaces a-Physicochemical and Engineering Aspects 137*(1-3):45−56. https://doi.org/10.1016/S0927-7757(97)00385-3

[16] Boussif O, Lezoualch F, Zanta MA, Mergny MD, Scherman D, Demeneix B, Behr JP (1995) A Versatile Vector for Gene and Oligonucleotide Transfer Into Cells in Culture and In-Vivo - Polyethylenimine. *Proceedings of the National Academy of Sciences of the United States of America 92*(16):7297−7301. https://doi.org/10.1073/pnas.92.16.7297

[17] Kim, EJ, Yeum JH, Ghim HD, Lee SG, Lee GH, Lee HJ, Han SI, Choi JH (2011) Ultrasmall Polyethyleneimine-Gold Nanoparticles with High Stability. *Polymer-Korea 35*(2):161−165. https://doi.org/10.7317/pk.2011.35.2.161

[18] Lee Y, Lee SH, Kim JS, Maruyama A, Chen XS, Park TG (2011) Controlled synthesis of PEI-coated gold nanoparticles using reductive catechol chemistry for siRNA delivery. *Journal of Controlled Release 155*(1):3−10. https://doi.org/10.1016/j.jconrel.2010.09.009

[19] Note C, Kosmella S, Koetz J (2006) Poly(ethyleneimine) as reducing and stabilizing agent for the formation of gold nanoparticles in w/o microemulsions. *Colloids and Surfaces A-Physicochemical and Engineering Aspects 290*(1-3):150−156. https://doi.org/10.1016/j.colsurfa.2006.05.018

[20] Sun XP, Dong SJ, Wang EK (2004) One-step synthesis and characterization of polyelectrolyte-protected gold nanoparticles through a thermal process. *Polymer 45*(7):2181−2184. https://doi.org/10.1016/j.polymer.2004.01.010

[21] Sun XP, Dong SJ, Wang EK (2005) One-step preparation of highly concentrated well-stable gold colloids by direct mix of polyelectrolyte and HAuCl4 aqueous solutions at room temperature. *Journal of Colloid and Interface Science 288*(1):301−303. https://doi.org/10.1016/j.jcis.2005.02.079

[22] Cho TJ, Gorham JM, Pettibone JM, Liu JY, Tan, JJ, Hackley VA (2019) Parallel multi-parameter study of PEI-functionalized gold nanoparticle synthesis for bio-medical applications: part 1—a critical assessment of methodology, properties, and stability. *Journal of Nanoparticle Research 21:188*. https://doi.org/10.1007/s11051-019-4621-3

[23] Cho TJ, Gorham JM, Pettibone JM, Liu JY, Tan JJ, Hackley VA (2020) Parallel Multiparameter Study of PEI-Functionalized Gold Nanoparticle Synthesis for Biomedical Applications: Part 2. Elucidating the Role of Surface Chemistry and Polymer Structure in Performance. *Langmuir 36*(46):14058−14069. https://doi.org/10.1021/acs.langmuir.0c02630

[24] Hackley VA, Clogston JD (2008) Measuring the Size of Nanoparticles in Aqueous Media Using Batch-Mode Dynamic Light Scattering. In *NIST - NCL Joint Assay Protocol PCC-1.* National Cancer Instititute, Nanotechnology Characterization Laboratory http://ncl.cancer.gov/working_assay-cascade.asp; http://dx.doi.org/NIST.SP.1200-6

[25] Cho TJ, Hackley VA (2018) Assessing the chemical and colloidal stability of functionalized gold nanoparticles. National Institue of Standards and Technology https://nvlpubs.nist.gov/nistpubs/SpecialPublications/NIST.SP.1200-26.pdf

[26] Schindelin J, Arganda-Carreras I, Frise E, Kaynig V, Longair M, Pietzsch T, Preibisch S, Rueden C, Saalfeld S, Schmid B, Tinevez JY, White DJ, Hartenstein V, Eliceiri K, Tomancak P, Cardona A (2012) Fiji: an open-source platform for biological-image analysis. *Nature Methods 9*(7):676−682. https://doi.org/10.1038/NMETH.2019

[27] Schneider CA, Rasband WS, Eliceiri KW (2012) NIH Image to ImageJ: 25 years of image analysis. *Nature Methods 9*(7):671−675. https://doi.org/10.1038/nmeth.2089

[28] Underwood SJ, Gorham JM (2017) Challenges and approaches for particle size analysis on micrographs of nanoparticles loaded onto textile surfaces. National Institute of Standards and Technology https://nvlpubs.nist.gov/nistpubs/SpecialPublications/NIST.SP.1200-22.pdf

[29] Cho TJ, Pettibone JM, Gorham JM, Nguyen TM, MacCuspie RI, Gigault J, Hackley VA (2015) Unexpected Changes in Functionality and Surface Coverage for Au Nanoparticle PEI Conjugates: Implications for Stability and Efficacy in Biological Systems. *Langmuir 31*(27):7673−7683. https://doi.org/10.1021/acs.langmuir.5b01634

[30] De Marzi L, Monaco A, De Lapuente J, Ramos D, Borras M, Di Gioacchino M, Santucci S, Poma A (2013) Cytotoxicity and Genotoxicity of Ceria Nanoparticles on Different Cell Lines in vitro. *International Journal of Molecular Science* 2013, 14(2): 3065-3077. https://10.3390/ijms14023065